Submitted to Journal of Chemical Thermodynamics

LBL-4903
Preprint

ENTROPY AND HEAT CAPACITY OF METHANE; SPIN-SPECIES CONVERSION

Gerald J. Vogt and Kenneth S. Pitzer

February 1976

Prepared for the U. S. Energy Research and Development Administration under Contract W-7405-ENG-48

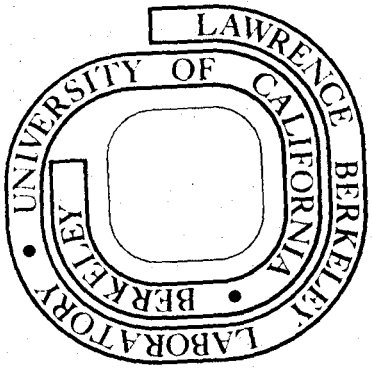

DISCLAIMER

Entropy and heat capacity of methane; spin-species conversion

Gerald J. Vogt and Kenneth S. Pitzer

Department of Chemistry and Materials and Molecular Research Division of the Lawrence Berkeley Laboratory, University of California, Berkeley, California 94720

(Abstract)

The heat capacity of methane from 0.4 to 28°K was measured for both pure methane and samples doped with about 0.8% oxygen as a spin-species conversion catalyst. With the conversion catalyst it was possible to obtain equilibrium with the spin system within about 30 minutes and to measure heat capacities down to 0.4°. For pure methane the spin-species conversion becomes very slow below 10°; however, one can measure non-equilibrium heat capacities on the basis of no change in spin-species composition. Entropy values are calculated from the heat capacities on the basis of both fixed and equilibrium spin-species composition and compared with the statistical calculation for gaseous methane. The results agree within possible experimental error with the expected zero point entropies for the two spin situations.

1. Introduction

The low-temperature properties of methane and its deuterated derivatives have long been of interest for their λ-transitions[1-4] associated, presumably, with the beginning of rotational disorder. With the extension of measurements into the liquid helium range, additional complications appeared[5] in the properties of methane which were later established as related to interconversion of nuclear spin species.[6-9] With four protons and tetrahedral structure there are three spin species of the following symmetry and total spin: A(I=2), T(I=1), E(I=0). The high-temperature distribution[10] is 5 A, 9 T, 2 E. Since the lowest rotational state, J=0, is allowed only for the A species, the equilibrium composition at 0°K will be 100% A for the gas and presumably also for the solid since some torsional motion will be allowed by quantum tunneling. In contrast to the behavior of ortho and para hydrogen, interconversion of spin-species in methane is rapid in the gas[11] because of degeneracies for higher states of different species. Interconversion rates decrease with decreasing temperature in the solid, and Colwell, et al,[5] were unable to measure equilibrium heat capacities below 5°. At that point the thermal relaxation time had become several hours.

This research was designed particularly to explore the thermal properties of methane below 5°K as well as to refine knowledge in related areas. It was hoped that by addition of a relatively high concentration of a paramagnetic species, the methane interconversion could be catalyzed and equilibrium measurements extended to much lower temperatures. About 0.8% oxygen proved to be a satisfactory catalyst. Equilibrium heat capacity measurements revealed a striking peak near 1°K which has been reported briefly.[12]

In this paper we present a full report on our experimental measurements together with their thermodynamic interpretation. Further discussion in terms of detailed models for the crystalline state will be presented elsewhere together with the details of our calculations related to the properties of oxygen in a methane lattice and the mechanism of the spin conversion catalysis.[13-15] Even for our present purposes, however, a brief summary of the present picture of the structure of crystalline methane is needed.

James and Keenan[16] proposed several structures for methane and analysed them on a classical basis more appropriate for CD_4 than for CH_4. Yamamoto, Kataoka, and others[17,18] have published an extensive series of papers on the quantum statistical-mechanics of methane in these structures. They conclude that methane below the λ-transition near 20°K has the "eight sublattice

antiferrorotational structure", which places three-fourths of the molecules in sites of D_{2d} symmetry while the remaining one-fourth are in sites of O_h symmetry.

The molecules in O_h sites will remain essentially disordered orientationally and have rotational energy levels similar to those for the gas; the lowest level has symmetry A; the next set of nine levels (J=1) at energy 12 to 15°K (estimated value of ε/k) are of symmetry T; while the 25 levels with J=2 include ten of E and fifteen of T symmetry and are at energy 30 to 45°K. With these relatively large energy separations, conversion preferentially to the A spin-species on cooling will begin above 10°K and will be nearly complete below 2°K. It is primarily this process that yields the rather high heat capacity near 6° observed by Colwell, et al.[5]

The molecules on the D_{2d} sites interlock with one another, as cog wheels, and their torsional energy level pattern will be collapsed and distorted from that of the gas. Kataoka, et al,[17] have developed an intermolecular potential for torsional motion which appears to fit our results very well. It yields at lowest energy a state of symmetry A and degeneracy 5 from spin. Next are a set of T states at about 1.9°K with total degeneracy nine followed by a doubly degenerate E level at about 2.8°K. Then there is a large energy interval between this array of "ground" torsional states and the librationally excited states above about 70°K.

Excitation of the molecules on D_{2d} sites from the lowest A state to the T and E states at 1.9 and 2.8°K, respectively, yields the heat capacity peak near 1°. In our earlier note we showed that our heat capacity data were well fitted on this model and obtained the more precise values of 1.951 and 2.89° for the A-T and A-E separations.

The statistical theory of Yamamoto, Kataoka, et al, considers the cooperative nature of these torsional phenomena, and this is important at higher temperatures; but below 2°K it is probably a good approximation to assume fixed energy separations as was indicated above.

There have also been extensive investigations of nuclear magnetic resonance[6-9] for solid methane which confirmed the interconversion of spin species below 10°K. We shall relate these results to our work in the paper to follow. Bloom and Morrison[19] have reviewed many topics related to solid methane.

2. Experimental Methods and Apparatus

The measurements were made in a calorimeter designed for use down through the helium -3 range to about 0.3°K. It is generally similar to that described by Finegold and Phillips.[20] The helium-3-cooled cryostat was inserted in a dewar system, consisting of two concentric glass dewars, the outer for liquid nitrogen and the inner with a pumpable jacket for liquid helium-4. The

pumping speed was such that the temperature of the helium-4 bath could be reduced to 1.1°K. In addition, the pumping system for the helium-4 bath was equipped with a pressure regulator so that the temperature of the bath could be controlled between 4.2° and 1.1°K.

The calorimeter and helium-3 chamber were enclosed in a vacuum can. Thermal contact could be established between the helium-4 bath and the helium-3 chamber and between the helium-3 chamber and the calorimeter by air-actuated mechanical clamps (heat switches). The helium-3 could be cooled from 1.1° to 0.3°K by reducing the vapor pressure.

The calorimeter was mechanically supported by monofilament nylon threads; also, the calorimeter was connected to the laboratory gas handling system by a thin-wall stainless steel capillary. This filling capillary and the electrical leads were thermally anchored to the helium-3 chamber before contacting the calorimeter.

The calorimeter, shown in figure 1, was constructed primarily of copper. The cylindrical section has a length of 37 mm, an internal diameter of 44 mm with a wall thickness of 1.0 mm and with an additional thickness of 0.6 mm at each reinforcing ring. The cylindrical section and the bottom dished end were one integral piece of metal. The dished ends had a wall thickness of 1.0 mm and a depth of 12 mm. Inside the cell a

spiral coil of 0.3 mm thick copper foil, uniformly spread over the volume of the cell, was thermally anchored to the outer wall to improve the thermal contact with a sample. Midway between the dished ends a copper screw was attached to the outer wall of the cell so that a bobbin wound with a heater coil could be readily connected to the calorimeter. In order to provide a means of attaching the thermometer to the cell, a piece of foil was soldered to the top dished end. A copper rod, 1.6 mm in diameter, was soldered to the outside of the calorimeter and was extended above the calorimeter to lie in between the jaws of the mechanical heat switch. All the pieces, including the top dished end, were silver-soldered together; the interior and exterior surfaces were gold-plated. The calorimeter had an internal volume of 79 cm^3 and a mass consisting of 125 gm of copper and 6 gm of other materials.

An encapsulated, four-lead doped Ge resistance thermometer[21] was attached to the calorimeter by rolling the thermometer in a foil soldered to the cell and using General Electric 7031 varnish for thermal contact and mechanical stability. To ensure good thermal contact with the cell, each lead from the thermometer was connected to a length of fine copper wire (0.3 mm diameter), wound and varnished in place about the copper cooling rod. To the other end of the fine copper wires

a free-standing coil of Pt-9% W wire 22 (0.06 mm diameter) was connected for thermal isolation. These coils were then connected to leads from the measuring circuit.

The Ge thermometer (Ge 782) was calibrated for the region 0.3° to 30°K on a temperature scale, designated T_η, in the laboratory of Professor Norman E. Phillips. The calibration was derived from a combination of Pt-resistance thermometry (T_{55}) between 15° and 30°K, gas thermometry between 4.2° and 20°K, the vapor-pressure of ^4He (T_{58}) between 4.2° and 1.1°K, and magnetic thermometry below 3°K with a single crystal of $Ce_2Mg_3(NO_3)_{12}\cdot 12H_2O$ (CMN).

The heater attached to the calorimeter was constructed by non-inductively winding and thermally anchoring with Stycast 2850GT a given length of Pt-9% W wire of 0.022 mm diameter upon the heater bobbin. The resistance of the heater, made from approximately 4m of wire, was 5470 Ω at 4.2°K.

The heat capacity of the empty calorimeter was measured several times over the temperature range of interest, 0.3° to 30°K. The contribution of the empty calorimeter to the total heat capacity was never over 50% and was less than 1% in the interesting region below 2.5°K for the samples containing oxygen.

The mass of calorimetric samples was determined by weighing in a small pressure vessel.[23] Since methane has a rather high freezing point, a special refrigerant

was needed for the transfer of a sample to the calorimeter without obstruction of the filling tube by a frozen plug. Natural gas, which is impure methane, served very well as this refrigerant; it was in turn liquified by use of liquid nitrogen.

Our pure methane was obtained from the Pacific Oxygen Company with a reported purity of 99.999%. Analysis in a mass spectrometer showed less than 5 ppm of O_2 or other impurity. Our samples of $CH_4 + O_2$ were intended to have about 1 mol% O_2. Some fractionation occurred in transfer to the calorimeter; hence each sample was analyzed by gas chromatography after calorimetric measurement. Table 1 gives the size and composition of the samples containing oxygen.

Some additional details concerning the apparatus are given elsewhere.[15]

Table 1. Samples of $CH_4 + O_2$

Sample No.	Sample Mass (gm)	O_2, mol%	Moles of CH_4*
100	6.380	0.68	0.3923_4
101	7.287	0.86	0.4465_6
102	6.561	0.85	0.4021_4
103	3.358	0.80	0.2060_2
104	2.671	0.87	0.1636_4

* Molecular weight of CH_4: 16.041 gm/mole.

3. Experimental Measurements

The heat capacity measurements were made by the usual heat pulse method. The effective surroundings of the calorimeter to which heat exchange took place was the helium-3 chamber and associated structure which will be called the "block". In the principal series of measurements reported in tables 2 and 3 the temperature of the block was controlled by one or another automatic temperature regulator; either a regulator of the vapor pressure of helium-3 or helium-4 or a regulated electrical heater yielding constant temperatures above the boiling point of helium-4. Prior to the use of these regulators, however, some measurements were made in which the block was allowed to drift thermally-presumably at a nearly constant temperature. Since there was no accurate measurement of block temperature in these preliminary measurements, their interpretation must be based entirely on calorimeter drifts and is somewhat uncertain. We report here in table 4 only those preliminary values that constitute an important supplement to the regular series with a regulated block temperature.

Interpretation of heat exchange corrections in this research was complicated by the slowness of thermal equilibration between the nuclear-spin-species conversion and the lattice-vibration energy. While we shall later discuss this situation for various temperature ranges for both pure and oxygen-doped methane, we consider first a general case and two limiting simplifications.

Table 2. Heat capacity of oxygen-doped methane

(1 cal = 4.184 J)

T	C(cal)
Sample 101	
1.5760	.5980*
1.6557	.5605*
1.8710	.4763*
2.0088	.4245
2.2451	.3795*
2.5230	.3556*
2.8135	.3397*
3.1661	.3410*
3.4410	.3446*
3.8261	.3540*
6.9561	.756
7.5233	.795*
7.7342	.824
8.3367	.904*
8.9974	1.013
Sample 102	
.70885	1.126*
.76893	1.142*
.84133	1.142*
.90087	1.106*
.93992	1.109*
.99886	1.071*

Table 2 (continued)

Sample 102 (continued)

1.08840	1.002*
1.20010	.904*
1.29690	.814*
11.43970	1.515*
12.63920	1.879
13.33050	2.047*
14.13900	2.368
16.51030	3.502
17.29090	4.069
18.02460	4.847
18.72100	6.071
21.10460	4.636
21.78720	4.685
22.52660	4.797
23.40100	4.908
24.38820	5.027
25.47220	5.234
26.65410	5.395

Sample 103

.45619	.6857*
.49313	.7955*
.50345	.8324
.51258	.8556
.52364	.8911
.53647	.9249

Table 2 (continued)

Sample 103 (continued)

.55029	.9585
.56482	.9984
.58028	1.0379
.59569	1.0750
1.41940	.7237*
1.46910	.6871
15.44560	2.9297
15.78360	3.0926
16.23700	3.3558
16.80160	3.7275
17.42920	4.2325
18.13600	5.0637
18.79120	6.3291
19.30150	8.9500
19.66840	13.12
19.91820	22.22
20.11720	24.60
20.64420	5.1927
21.58640	4.7151
22.66070	4.8224
23.81110	4.9660
25.07940	5.1890
26.40630	5.4125
27.76710	5.4809

Table 2 (continued)

T	C(cal)
Sample 104	
.43673	.603*
.43744	.604*
.44461	.633
.44796	.657
.45327	.665
.46001	.691
.46319	.699
.47276	.734
.47427	.740
.48641	.779
.48765	.780
.49947	.819
.50281	.838
.51123	.856
.52497	.895
.53920	.942
.56771	1.008
.58067	1.039
.59560	1.062
.62389	1.101
.64427	1.131
.66558	1.169
.68774	1.195
.70877	1.200
.72915	1.214

Table 2 (continued)

T	C(cal)
Sample 104 (continued)	
.75262	1.217
.77991	1.219
.81133	1.205
.84733	1.188
.87870	1.169
.90186	1.163
.92699	1.142
.95467	1.120
.98463	1.093
1.01860	1.066
1.05590	1.035
1.09570	.999
1.13890	.954
1.18600	.912
1.23960	.857
1.30190	.806
1.37250	.749
1.44740	.696
1.52740	.645
6.38800	.715
6.87600	.744
7.10870	.761
7.5268	.837
7.8374	.859

Table 2 (continued)

T	C(cal)
Sample 104 (continued)	
8.2514	.925
8.6723	.991
9.1150	1.066
9.6040	1.143

* These values may be slightly too small; reason given in text.

Table 3. Heat capacity of pure methane

(1 cal = 4.184 J)

Non-Equilibrium Data

T	C(cal)
Series 9	
5.9835	.178
6.9203	.284
8.0141	.449
9.9042	.793
Series 14A	
2.1945	.00381
2.2338	.00404
2.3238	.00439
2.4174	.00496
2.4855	.00539
2.5321	.00555
2.5378	.00587
2.6051	.00640
2.6750	.00704
2.7503	.00780
2.9013	.00960
2.9314	.01007
3.0055	.01097
3.1107	.01259
3.2046	.01412
3.3008	.01587
3.3997	.01834

Table 3 (continued)

Series 14A (continued)

T	C(cal)
3.4425	.01848
3.5442	.02067
3.7191	.02479
3.7880	.02698
3.9253	.03036

Series 14B

4.3029	.0382
4.5015	.0463
4.7078	.0559
4.8996	.0652
5.0945	.0761
5.2832	.0879
5.4318	.0988
5.6000	.1128
5.7705	.1271
5.9444	.1435
6.1294	.1620
6.2856	.1804
6.4343	.1997
6.6152	.2226
6.7438	.2431
6.8989	.2651
7.1134	.2955
7.2737	.3213

Table 3 (continued)

Series 14B (continued)

T	C(cal)
7.5524	.3607
7.9043	.4143
8.2415	.4717
8.6328	.5367
9.1080	.6273
9.6137	.7269

Series 14C

4.4985	.0575
4.5898	.0612
5.3604	.1072
5.6860	.1367
7.9392	.4257
9.8450	.7723

Series 14D

21.4026	4.599
22.7433	4.738
24.5678	4.976
26.5792	5.295
28.7184	5.581

Table 3 (continued)

Series	T	C(cal)
	Equilibrium Data	
14C	7.7669	0.801
13	7.9301	.855
14C	9.7402	1.114
13	9.8299	1.143
7	10.8742	1.305
13	11.3526	1.407
7	11.9787	1.5541

Table 4. Additional heat capacity measurements for methane

(1 cal = 4.184 J)

T	C(cal)
Sample 100; Oxygen-doped	
2.3706	0.366 ± 0.03
3.0316	.411 ± .07
4.2448	.371 ± .05
4.4105	.458 ± .09
4.6907	.463 ± .08
5.0129	.497 ± .08
5.3223	.555 ± .08
5.7910	.596 ± .08
6.2778	.633 ± .06
6.8211	.716 ± .05
7.1847	.736 ± .01
7.7809	.910 ± .06
8.2777	.928 ± .02
8.8695	1.009 ± .01
9.5878	1.146 ± .01
10.2155	1.230 ± .02
10.9945	1.399 ± .01
12.1089	1.676 ± .01
13.2824	2.002 ± .02
14.0669	2.238 ± .03
15.5121	2.871 ± .01

Table 4 (continued)

T.	C(cal)
Series 4, pure methane	
15.2513	2.486
15.6139	2.661
16.0344	2.847
16.3216	2.930
16.6564	3.154
16.9764	3.363
17.3723	3.611
17.7299	3.922
18.0576	4.067
18.3962	4.619
18.7506	4.999
18.7529	4.904
19.2247	5.877
19.7119	7.164
20.2213	10.511
20.4810	52.044

Table 4 (continued)

T	C(cal)
Series 5, pure methane	
15.1314	2.365
15.7982	2.662
16.3325	2.946
16.3319	2.958
16.9308	3.305
17.4869	3.654
17.9209	4.032
18.3343	4.459
18.7540	4.976
19.0861	5.472
20.9891	4.522
21.5709	4.510
22.2748	4.592
23.1684	4.702

The calorimeter is assumed to reach rapid thermal equilibrium with the lattice energy of the methane. There remains, then, slow heat transfer with rate constants k_B and k_s respectively with the block at temperature T_B and the nuclear spin system at temperature T_s. In general the calorimeter temperature drift after a heating interval will be governed by the equation

$$C \frac{dT}{dt} = \dot{q} = k_B(T_B-T) + k_s(T_s-T) \qquad (1)$$

where t is the time, C is the heat capacity of the calorimeter plus methane lattice and $\dot{q}$ is the rate of heat flow into that system.

If the heat transfer from the spin system is either negligibly slow or so rapid that it has already attained equilibrium, the last term in equation (1) can be omitted and the remainder integrated, with T_B constant, to yield.

$$T = T_B + (T_o-T_B) \exp(-k_B t/C) \qquad (2)$$

Here T_o is the temperature at zero time. If the spin system is in equilibrium, C includes the spin heat capacity. If the exponent is small, this approximates to a linear equation which was found to be adequate in most but not all cases.

Another simplifed case arises if the heat exchange with the block can be neglected. In this case we cannot assume T_s constant; rather it will vary in accordance with heat transfer and the spin-related heat capacity C_s which can be taken to be constant for a given measurement. After considerable manipulation one obtains

$$T = \frac{CT_{s,o}+C_sT_o}{C+C_s} + \frac{C(T_o-T_{s,o})}{C+C_s} \exp\left(-\frac{k_s(C+C_s)t}{C^2}\right) \qquad (3)$$

where $T_{s,o}$ is the spin-system temperature at zero time. This equation is seen to have the same general form as equation (2). In either case the logarithm of the drift rate, log(dT/dt), decreases linearly with time and one can extrapolate to find T_o. But if equation (3) is assumed, the extrapolation also yields an unchanged spin temperature at zero time.

While we have a few examples where both terms on the right side of equation (1) are comparably important at some time during the after drifts, it did not seem worthwhile to attempt to interpret these data in terms of a general integration of that equation. In these cases the heat transfer to the spin system dominated the early drifts while the late drifts were well-fitted on the basis of a small heat transfer with the block after equilibration with the spin system.

Any errors arising from energy and temperature measurements should not lead to errors in heat capacities exceeding 1% which is less, in most regions, than the uncertainty arising from interpretation of the after drifts.

Let us now turn to a discussion of the actual results in various temperature regions. For oxygen-doped methane we always obtain equilibrium with the spin system but in some cases only after about 30 minutes. Colwell, et al,[5] reported equilibration times of several hours near 5°K for a sample containing 50 ppm oxygen. In all cases the temperature history included about 10 hrs at 4.2°K after initial cooling with helium-4; also the calorimeter was sometimes held over-night at that temperature between sets of measurements. For work below 1.5°K the calorimeter was cooled by use of helium-3 and measurements followed immediately after equilibration.

For the first heat capacity measurement after rapid cooling there is always some additional uncertainty about thermal equilibration before the heat input. This is especially likely to be a problem in the region below 6° where equilibration is very slow with the spin system. The effect would be to yield too low a heat capacity since the initial spin energy would be higher than the equilibrium value for the initial temperature. All measurements of this type below 6°, i.e., immediately preceded by cooling, are marked with an asterisk in

table 2. Those in series 102 below 1.0° are definitely too low and are omitted from figure 2. It is not clear that others are in error, but the entire series from 1.5 to 4.0° are subject to this error and may indicate too low a curve in figure 3.

The most interesting result is the peak in the heat capacity near 0.8°K shown in figure 2 and concerning which a preliminary report[12] has been published. Although this is a region of slow equilibrium the measurements are apparently reproducible within a single series to within ± 1%. However, as just discussed, lack of perfect thermal equilibration can lead to uncertainties somewhat larger than 1%.

In the 2-10° region shown in figure 3 the heat capacity continues to show a spin-related contribution, but the lattice contribution increases rapidly and dominates near 10°K. The heat capacity in the 2-5° region is rather small, equilibrium is still slow, and the results are less accurate than below 2°. Between 4 and 6° we have only measurements from the less accurate preliminary series without block regulation. The estimated uncertainty, which is given for each value in table 4 for this series, is based on the range of reasonable interpretations of the after drifts. Several of these early points overlap the region of more accurate measurement above 6°. In this range the agreement is good enough to support the validity of

the results from 4 to 6°K. The results of Colwell, et al,[5] begin near 5° and agree quite well with our data up to 10°.

We turn now to the data for pure methane below 10°K. The behavior of pure methane was explored by cooling for 9 hr at 1.1°K and then breaking the thermal contact (by the heat switch). The calorimeter temperature rose rapidly to 2.0° in 10 minutes and reached 2.3° in an hour. After another 6 hr cooling at 1.1° and again breaking thermal contact, the calorimeter temperature again rose rapidly to 2.0° and approached 2.2° after two hours. It was impractical to make heat capacity measurements in this temperature range because the lattice heat capacity is so small that the heat flow from the spin system dominates the situation.

Beginning at about 2.2°K one can measure the "non-equilibrium" heat capacity of the lattice system alone by extrapolation of the after drifts with equation (3) which considers the heat transfer from the spin system. Although this extrapolation removes the heat capacity arising from change in spin-species composition, it does not determine the spin-species composition or the equivalent spin temperature. Since there is at least some rotational or librational contribution to the "lattice" heat capacity which will be different for different spin species, there is some residual indeterminancy associated with these non-equilibrium heat capacities.

Figures 4 and 5 show the non-equilibrium results for the 2-4° and 4-10° regions, respectively, together with the results of Colwell, et al.[5] The results of the two investigations agree reasonably well near 2.3°K and again near 6.5°, but the data of Colwell, et al, are considerably higher than ours from 3.5 to 6° while they are significantly lower from 7.5 to 10°K. On the basis of the model of Kataoka, et al,[17] we have made rough calculations of the librational heat capacity for various spin-species distributions. This effect is very small at 2°K, but rises rapidly for the T (and E) spin-species.[24] For the A spin-species the librational heat capacity becomes significant only about 6°K.

Before the series 14B measurements the sample had been held below 4.2°K for a very long time while the series 14A measurements were made and between series 14A and 14B. On the other hand the sample had been heated above 18°K prior to cooling again to 4.2° for 11 hr prior to series 4C. The heat capacity values in series 4C are a little larger than those in series 4B which would agree with a higher spin temperature (more species T and E) in series 4C. Presumably, if the sample had been held an even shorter time at 4.2°K, even higher heat capacities would have been obtained. Hence, if Colwell, et al,[5] did not hold their sample as long below 4.2° as we did, they would have had more T (and E) species remaining and their higher heat capacities from 3.5 to 6° are understandable.

In the vicinity of 6°K the rate of spin-species conversion becomes large enough that the spin temperature will not differ much from the lattice temperature at the beginning of a heat capacity measurement. Correspondingly, the extrapolation of after drifts becomes more uncertain. At slightly higher temperatures one obtains after drifts such as are shown on figure 6. There are two regions in which the log (dT/dt) is linear in t. In the earlier period presumably the spin relaxation dominates and one may apply equation (3) to yield the non-equilibrium heat capacity while in the later period one assumes spin equilibrium and that equation (2) may be applied for heat transfer to the block to yield an equilibrium heat capacity. There are five examples between 7.5 and 10°K for which both equilibrium and non-equilibrium heat capacities were derived and listed in separate sections of table 2.

Above 10°K measurements on both pure methane and the oxygen-doped samples yield equilibrium heat capacities shown on figures 7 and 8. Our only values for pure methane are from preliminary series without temperature regulation of the block. We report these in table 4 only above 15°K where complete thermal equilibrium after heating is reasonably rapid. As can be seen on figure 8 our results for pure methane agree with those of Colwell, et al, above 18°, but below that temperature our results are slightly lower (and our unreported results below 15° depart even further on the low side).

Our results for oxygen-doped methane (which were made with temperature regulation of the block), are higher than those from either research for pure methane by an amount which increases from 10°K toward the transition near 20°. Above the transition all results agree quite well.

The λ-type transition near 20°K was investigated in two ways in addition to the heat capacity data shown on figure 8 and recorded in the tables. Integral heating experiments were performed in which the sample is heated from about 19 to 21°K. The results are given in Table 5 for the exact temperature interval for each experiment. Also given is the integral heat converted to the interval 19.0 - 21.0° by use of heat capacity data.

In addition the temperature was observed while heating through the transition and an essentially constant temperature was observed for an appreciable time. For pure methane this apparent temperature of transition was found to be 20.53°K. Colwell, et al,[5] measured this temperature by heating into the transition and then measuring the temperature at zero heat input. They found 20.49°; the difference of 0.04° could easily be caused by thermal gradients in our experiment. We shall use Colwell's value for our calculations. Sperandio[25] reported 20.55° for this transition temperature in reasonable agreement with the other values.

Table 5. Enthalpy change for the λ-transition

(1 cal = 4.184 J)

Temperature range T_1	T_2	$\Delta H(T_1 \rightarrow T_2)$ (cal/mole)	$\Delta H(19.5 \rightarrow 21.0°)$ (cal/mole)
		Pure methane	
19.251	20.654	21.949	22.27
18.427	20.929	27.847	22.36
18.819	21.300	27.753	22.45
		average	22.36 ± 0.1
		Oxygen-doped methane	
19.557	21.265	19.167	18.55
19.417	20.778	17.627	17.84
18.681	20.793	23.451	18.08
18.746	20.834	23.369	18.18
		average	18.17 ± 0.3

For oxygen-doped methane we obtained 20.30°K for the transition temperature which is 0.23° lower than that for pure methane. Also note that the heat of transition $\Delta H(19 \rightarrow 21°)$ is 4.2 cal/mole less whereas the heat capacity below 19° is considerably larger for the oxygen-doped sample than for pure methane.

In this connection it is interesting to note the results of Eucken and Veith[26] for krypton mixtures with methane. For a sample with 3.70 mol% Kr the λ-transition has shifted down in temperature by 1°K and the heat capacity of the mixture below the transition

has increased considerably as for our oxygen mixtures. The height of the transition has, however, decreased significantly from some 80 cal/deg-mole to under 20 cal/deg-mole. For further increases of the krypton concentration the transition shifted to lower temperatures and generally broadened until the transition was no longer detected at 32 mol% Kr.

Thus, it seems plausible that the introduction of the oxygen impurities (0.8 to 0.9 mol%) has so affected the intermolecular forces that the λ-transition has been shifted down in temperature and broadened.

Since the heat capacity for pure methane and the oxygen-doped samples agree to within experimental uncertainty at 9°K and 28°K, with considerable disparity between these temperatures, the changes in enthalpy and entropy between 9° and 28°K were computed and compared. The following results were obtained:

	$\Delta H(9° \rightarrow 28°K)$ (cal/mole)	$\Delta S(9° \rightarrow 28°K)$ (cal/deg-mole)
$CH_4 + O_2$..	84.80 ± 0.30	4.368 ± 0.014
Pure CH_4..	84.85 ± 0.21	4.341 ± 0.005

The enthalpy increments are indeed nearly equal, but the value for the oxygen-doped samples should have some contribution from the oxygen. As determined from the free molecule model for an additive oxygen heat capacity, the dissolved oxygen could possibly contribute as much as 0.38 cal/mole. Taking this estimate into account, the two values of $\Delta H(9° \rightarrow 28°K)$ still agree to within 0.5%.

The entropy increments likewise tally with each other quite closely.. In this case, the maximum additive contribution by oxygen is 0.021 cal/deg-mole for the free molecule model. With this correction $\Delta S(9°\rightarrow 28°K)$ for the $CH_4 + O_2$ sample remains slightly higher by 0.14%. Seemingly, despite the considerable effect of the dissolved oxygen on the λ-transition, the over-all change in enthalpy and entropy for the affected region remains the same within experimental uncertainty.

4. Entropy Comparisons; Discussion

As indicated in the introduction, we shall present here the calculations of experimental entropy differences based upon our experimental data and make comparisons with gas-phase statistical calculations of the entropy and zero-point entropy values for appropriate models. We leave to another place the discussion of our results in relation to more detailed statistical calculations for the solid state.

For comparison we recalculated the statistical entropy of methane in the ideal gas state using the usual equations[27] with recent constants and molecular parameters.[28,29] The result for 298.15°K and 1 atm is 44.51 cal/deg-mole on the practical basis excluding nuclear spin. This does not differ significantly from literature values, for example a 1944 calculation[30] reported 44.50. This statistically calculated entropy for the gas remains the best value for use in thermodynamic

calculations. If nuclear spin entropy is included this is increased by R ℓn 16 = 5.51 cal/deg-mole to yield a total of 50.02. For calculations related to the experimental measurements on liquid methane a convenient set of conditions is 99.54°K and 246.1 Torr or 0.3238 atm. The statistical entropy without nuclear spin for these conditions is 37.93 cal/deg-mole.

We shall use as a basis of comparison the entropy of the liquid at 21.0°K. The experimental data on solid methane above this temperature and on the liquid are uncomplicated by the peculiarities at lower temperatures and are quite accurately known.[1,5,25] Literature values for the heats of fusion and vaporization are given in table 6. There is good agreement for the heat of fusion. The calorimetric heat of vaporization of Clusius and Frank[4b] agrees well with that calculated from the vapor pressure equation by the exact Clapeyron equation. The liquid[31] and vapor[32] volumes are accurately known; hence this calculation has high reliability. The equation of state of the vapor also yields an accurate correction from the ideal to the real gas. The equation of Pitzer and Curl[33] with parameters for methane from Pope, et al,[32b] yields -0.05_7 cal/deg-mole while the equation of McGlashan and Potter[32a] yields -0.05_3. Other equations[34,35] which should yield a good approximation for methane confirm a value near -0.06 (which differs from the value -0.14 adopted without explanation by Colwell, et al.[5]) The result for the entropy of solid methane at 21° is given in table 7.

Table 6. Heats of fusion and vaporization for methane

Heat of fusion: T_{TP} = 90.67°K

Source	Temperature Range (°K)		ΔH_f (cal/mole)
Sperandio[25]	87.62	92.32	225.63
	87.20	90.91	224.72
	88.70	93.44	225.15
Clusius[1]	89.20	90.92	225.7
	90.15	91.92	222.3
	88.33	95.27	224.5
	88.71	93.49	223.3
Average			224.4_7

Heat of vaporization: T = 99.54°K, P = 246.1 torr

Source	ΔH_{vap} (cal/mole)
Clusius and Frank[4b]	2036 ± 2
Calculation from vapor pressure data	2037.5

Table 7. Calculated entropy of solid methane at 21°K from data at higher temperatures in cal/deg-mole

S° ideal gas at 99.54°, 0.3238 atm	37.93
Correction to real gas	- .06
Condensation 2037/99.54	-20.46
Liquid heat capacity	- 1.21
Solidification	- 2.48
Solid heat capacity	-10.66
S° solid at 21.0° (without nuclear spin)	3.06

For most substances the nuclear-spin species distribution remains unchanged down to the lowest temperature of heat capacity measurements; then the usual equations and third law of thermodynamics yield an entropy value excluding nuclear spin. Use of the non-equilibrium heat capacities for methane (or extrapolation from above 12°K) should yield an approximation to this case for methane, but there are complicating factors to be discussed. Figure 9 shows a selection of pertinent data below 20°K presented as C/T values whose integral yields the entropy. We show the values of Colwell et al,[5] from 12 to 20° since we believe their data are probably better than ours in this range. Below 10° we show our values from series 13 and 14C together with a few points from Colwell, et al. The entropy values corresponding to several curves through this region are given in table 8.

Table 8. Entropy of methane at 19.5°K on the basis of frozen spin-species composition

$S_{21.0}$ from table 7 (cal/deg-mole)	3.06
Subtract S(trans) = 22.36/20.49	-1.09
$S_{19.5}$ from data at higher temperature	1.97
$S_{19.5}$ from "best curve" below 19.5°	1.93
$S_{19.5}$ from Debye function (θ_D = 72.8) plus experimental curve above 12°	2.06
$S_{19.5}$ from pure methane data of this research	1.81

Parenthetically we first note that if one had data only above 12°K, as is typical when liquid hydrogen is the refrigerant, one would find an excellent fit with the Debye function in the region 12-14° with $\theta_D = 72.8$. Then if one adds the Debye entropy at 12° to that for the experimental curve above 12°, the result at 19.5° is 2.06 which slightly exceeds the value of 1.97 calculated from the statistical entropy of the gas and experimental data above 19.5°. This calculation yields agreement to better than 0.1 cal/deg-mole which one would interpret as quite satisfactory since either the extrapolation below 12° or the value based on data at higher temperatures could be in error by 0.05 and possibly by 0.1 cal/deg-mole. While the data then available were slightly less accurate in some regions, the situation remained substantially as stated above until the measurements were extended into the liquid helium range.

Next we note that a straightforward calculation based upon our non-equilibrium heat capacities below 10°K and our pure-methane data above 10° yields $S_{19.5} = 1.81$ which is too small by 0.16. Although these data yield a reasonably smooth curve (not shown on figure 9), we believe this is accidental. The higher values of Colwell, et al, are to be preferred above 10° because in this region our data are not based on a controlled block temperature. Below 10° our experimental quality is excellent, but there is a variation of result

with thermal history which indicates that the spin-species composition is varying and affects the heat capacity.

We show as a solid line on figure 9 our estimate of the true heat capacity for frozen spin-species composition. This is based on the non-equilibrium data near 2° but rises above the non-equilibrium values from 3 to 10° by an amount calculated from estimates about the spin-species composition and its effect on the librational heat capacity calculated from the model of Kataoka, et al.[17] Near 12° the heat capacity is reduced from the measured equilibrium value by an amount similarly calculated for change in spin-species composition. This last correction decreases rapidly with rising temperature. The entropy based on this "best curve" is 1.93 at 19.5° in good agreement with the value 1.97 derived from data at higher temperatures.

There is an interesting theoretical possibility that the remaining entropy at 0° on the frozen spin species basis may not be exactly R ℓn 16. This situation is discussed in an Appendix.

It is now interesting to re-examine figure 8. The solid curve is our best estimate of the true heat capacity with the spin-species composition frozen at the high-temperature pattern. The Debye extrapolation curve is too high below 15° and the fit in the 12-15° region is accidental since the experimental data include a small contribution from spin-species conversion.

Also shown for comparison on figure 9 is a dashed curve for C = (const) T^3 fitted in the 16-18° range. Actually, the fit to the T^3 curve in the 16-18° range is accidental since the λ-transition is beginning to have some effect here.

We turn now to consideration of the equilibrium heat capacity curve below 10°K including our data for oxygen-doped methane. For our comparison we add the nuclear spin entropy R ℓn 16 = 5.509 to our earlier value for the entropy at 21.0° obtaining 8.57 cal/deg-mole. Also the expected zero point entropy on this basis is R ℓn 5 = 3.198 since all of the methane will be converted to the A spin-species with spin I=2 and $g_o = 2I+1$.

The various increments in this calculation are shown in table 9. The extrapolation below 0.44° is calculated from the energy-level pattern given above which fits the heat capacity peak near 1°. The entropy introduced in spin-species redistribution for the molecules at D_{2d} sites is (3/4) R ℓn (16/5) = 1.733. It may be noted that this is approximately the entropy at 3°. Since the heat capacity remains above 0.3 cal/deg-mole at its minimum near 3°, there is considerable overlap between the peak near 1° associated with the spin-species redistribution for the methane on D_{2d} sites and the high heat capacity in the 4-6° region associated with the redistribution for that on O_h sites. Lattice heat capacity also begins to be significant above 2°;

hence there is no distinct peak associated with the spin for the O_h sites.

Table 9. Entropy including nuclear spin for solid methane (in cal/deg-mole).

0-0.44°K (Extrapolation)	0.167
0.44 - 3.0°	1.52 ± .05
3.0 - 19.5	2.66 ± .05
19.5 - 21.0 transition 18.17/20.30	$.89_5$
Zero point entropy, R ℓn 5	3.198
$S_{21.0}$ (sample containing 0.8% O_2)	8.44
Estimated entropy of O_2	- .06
$S_{21.0}$ For pure methane	8.38
$S_{21.0}$ From higher temperature data	8.57

The comparison with the entropy integrated from our heat capacity data for oxygen-doped methane is shown in table 9.

Furthermore, the oxygen impurity must contribute some entropy which should be subtracted from the 8.44 value in table 9. We have estimated this correction for the oxygen[15] to be 0.06 ± .02 which increases the difference shown in table 9 to 0.19 cal/deg-mole. This discrepancy is at the upper limit of experimental error for all of the increments included in table 7 as well as table 9 and seems improbably but not impossibly large. However, it is also possible that the oxygen was not uniformly distributed in our doped samples when crystallized and that a small portion of the methane

failed to attain spin-species equilibrium at very low temperatures. If this last-stated situation arose, it could explain part or all of the entropy difference between the two values for $S_{21.0}$ in table 9, and in that case our heat capacities in the spin-species conversion region below about 6° should be increased slightly.

In conclusion, it appears that the various peculiarities in the low-temperature thermal properties of methane are now understood in terms of spin-species composition which becomes frozen below about 10°K unless catalyzed with paramagnetic molecules such as oxygen. With the catalyst present the methane converts to species A with a zero-point entropy of R ℓn 5. Without the catalyst the methane retains most of its total nuclear spin entropy of R ℓn 16. The detailed shape of the spin-equilibrium heat capacity curve, including the peak near 1°K, is generally consistent with the model presented by Kataoka, Okoda, and Yamamoto,[17] but we await with interest calculated heat capacities based on full use of their theory including cooperative effects.

This research was sponsored by the Energy Research and Development Administration.

5. Appendix

When methane is cooled without a spin-species conversion catalyst some species T and E molecules will remain at 0°K. On the assumption of the eight-sublattice antiferrorotational structure as discussed by James and Keenan[16] and by Kataoka, et al,[17] the zero-point degeneracy is 5 for the A species and 9 for the T species for either the D_{2d} or O_h sites without ambiguity. Also for the E species the degeneracy is clearly 2 at the D_{2d} sites, but at the O_h sites the E molecules are expected to have a 6-fold degeneracy in their lowest energy level. This is shown most clearly by Nishiyama and Yamamoto[18] for a methane molecule in a rare gas lattice with sites also of O_h symmetry. Kataoka, et al,[17] indicate a similar pattern for the E species at the O_h sites in solid methane. Our extrapolation below 2° implied by the "best curve" of figure 9 and table 8 relates to a state including some E molecules on O_h sites. If we take the high-temperature fraction of such molecules, (1/4) x (2/16) = 1/32, the extra zero-point entropy (above the R ℓn 16 for proton spin) would be (1/32) R ℓn(6/2) = 0.07 cal/deg-mole on the basis of the 6-fold degeneracy for the E species on O_h sites. This value is of the same sign and slightly larger than the difference (1.97-1.93) shown in table 8, but the uncertainty in these experimental values is too large to make this comparison really significant.

REFERENCES

1. Clusius, K. Z. Physik. Chem. 1929, B3, 41

2. Clusius, K; Perlick, A. Z. Physik. Chem. 1934, B24, 313.

3. Clusius, K; Popp, L; Frank, A. Physica 1937, 4, 1105.

4. (a) Frank, A; Clusius, K. Z. Physik. Chem. 1937, B36, 291.
(b) Ibid 1939, B42, 395.

5. (a) Colwell, J. H.; Gill, E. K.; Morrison, J. A. J. Chem. Phys. 1962, 36, 2223.
(b) Ibid, 1963, 39, 635.

6. Wolf, R. P.; Whitney, W. M. Proceedings of the Ninth Conference on Low Temperature Physics (Plenum Press, 1965), 1118.

7. Hopkins, H. P.; Donoho, P. L.; Pitzer, K. S. J. Chem. Phys. 1967, 47, 864.

8. Wong, K. P.; Noble, J. D.; Bloom, M.; Alexander, S. J. Magn. Resonance 1969, 1, 55.

9. van Hecke, P.; Grobet, P; van Gerven, L. (a) Phys. Lett. 1970, 33A, 379; (b) J. Magn. Resonance 1972, 7, 117; (c) Physica 1973, 68, 359.

10. Wilson, E. B. J. Chem. Phys. 1935, 3, 276.

11. Curl, Jr., R. F.; Kasper, J. V. V.; Pitzer, K. S. J. Chem. Phys. 1967, 46, 3220.

12. Vogt, G. J.; Pitzer, K. S. J. Chem. Phys. 1975, 63, 3667.

13. A preliminary presentation of this material may be found in the theses of Janice J. Kim and Gerald J. Vogt-references 14 and 15, respectively.

14. Kim, J. J., Ph.D. Thesis, University of California, 1975; also Lawrence Berkeley Laboratory Report LBL 3955.

15. Vogt, G. J., Ph.D. Thesis, University of California, 1976, also Lawrence Berkeley Laboratory Report LBL 4149.

16. James, H. M.; Keenan, T. A. J. Chem. Phys. 1959, 31, 12.

17. Kataoka, Y.; Okada, K; Yamamoto, T. Chem. Phys. Lett. 1973, 19, 365.

18. Nishiyama, K; Yamamoto, T. J. Chem. Phys. 1973, 58, 1001 and earlier papers there cited.

19. Bloom, M.; Morrison, J. A. Orientational Order and Disorder in the Solid Isotopic Methanes in Surface and Defect Properties of Solids (Specialist Periodical Reports of the Chemical Society, London, 1973), 2, 140.

20. Finegold, L.; Phillips, N. E. Phys. Rev. 1969, 177, 1383.

21. Cryocal, Inc., Riviera Beach, Florida.

22. Ho, J; Phillips, N. E. Rev. Sci. Instr. 1965, 36, 1382.

23. Finegold, L. J. Sci. Instr. 1967, 44, 789.

24. See reference 15, pp. 149-153.

25. Sperandio, A. Thesis, University of Zurich, 1961.

26. Eucken, A.; Veith, H. Z. Phys. Chem. 1936, B34, 275.

27. Pitzer, K. S.; Brewer, L. revision of "Thermodynamics" by G. N. Lewis and M. Randall, Chapter 27, McGraw-Hill Book Co., New York, 1961.

28. Herzberg, G. Molecular Spectra and Molecular Structure II. Infrared and Raman Spectra of Polyatomic Molecules (Van Nostrand Co., New York, 1945), p. 307.

29. Herranz, J.; Stoicheff, B. P. J. Mol. Spectry. 1963, 10, 448.

30. Pitzer, K. S. Ind. Eng. Chem., 1944, 36, 829.

31. Terry, M. J.; Lynch, J. T.; Bunclark, M.; Mansell, K. R.; Staveley, L. A. J. Chem. Thermo. 1969, 1, 413.

32. (a) McGlashan, M. L.; Potter, D. J. B. Proc. Roy. Soc. (London) 1962, A267, 478

(b) Pope, G. A.; Chappelear, P. S.; Kobayashi, R. J. Chem. Phys. 1973, 59, 423.

33. Pitzer, K. S.; Curl, Jr., R. F. J. Amer. Chem. Soc. 1957, 79, 2369.

34. see Dymond, J. H.; Smith, E. B. The Virial Coefficients of Gases: A Critical Compilation (Oxford, Clarendon Press, 1969), pp. 26-31.

35. Douslin, D. R.; Harrison, R. H.; Moore, R. T.; McCullough, J. P. J. Chem. Engr. Data 1964, 9, 358.

FIGURE CAPTIONS

Figure 1. Diagram of the calorimeter.

Figure 2. Equilibrium heat capacity of methane (doped with oxygen) below 1.7°K.

Figure 3. Equilibrium heat capacity of methane from 1 to 10°K. Open circles are for methane doped with oxygen; solid circles for pure methane.

Figure 4. Non-equilibrium heat capacity of methane (with frozen spin-species composition) from 2 to 4°K.

Figure 5. Non-equilibrium heat capacity of methane from 4 to 10°K; see text for discussion of spin-species composition for various measurements.

Figure 6. After drifts showing two regions where $\log (\Delta T/\Delta t)$ is linear in time.

Figure 7. Equilibrium heat capacity of methane from 10 to 17°K.

Figure 8. Heat capacity of methane in the region of the transition near 20°K.

Figure 9. Entropy for non-equilibrium methane from C/T vs T plot; see text for explanation of various curves.

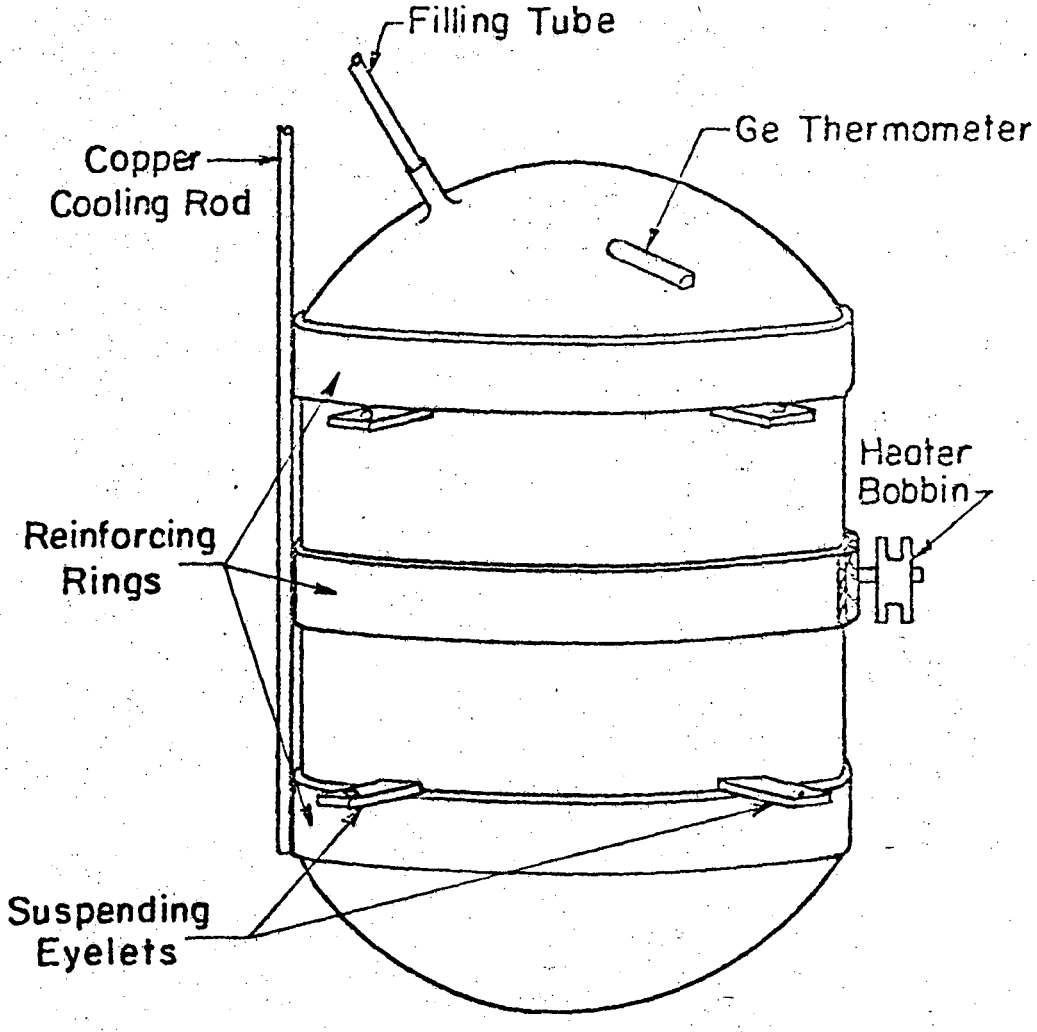

Figure 1. Diagram of the calorimeter.

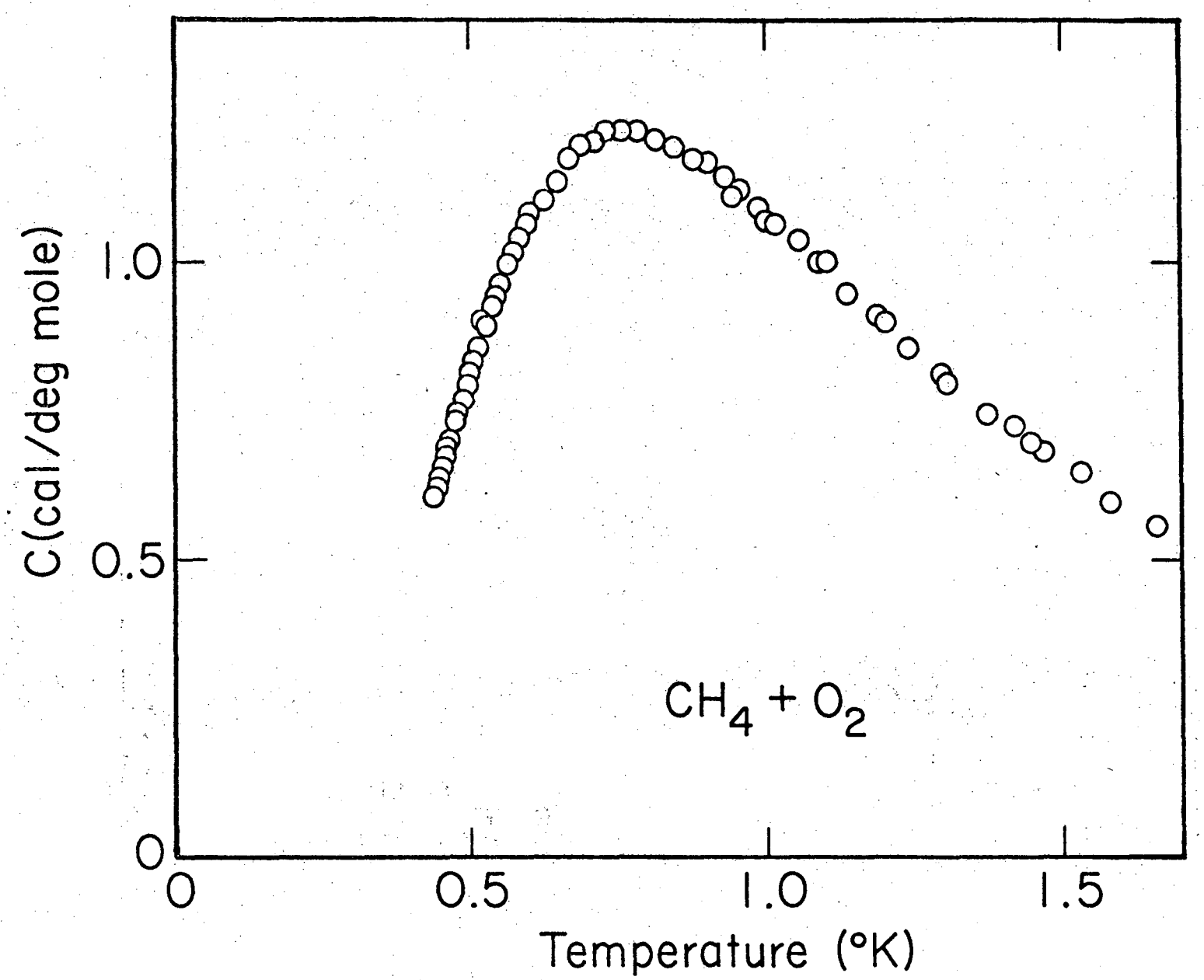

Figure 2. Equilibrium heat capacity of methane (doped with oxygen) below 1.7°K.

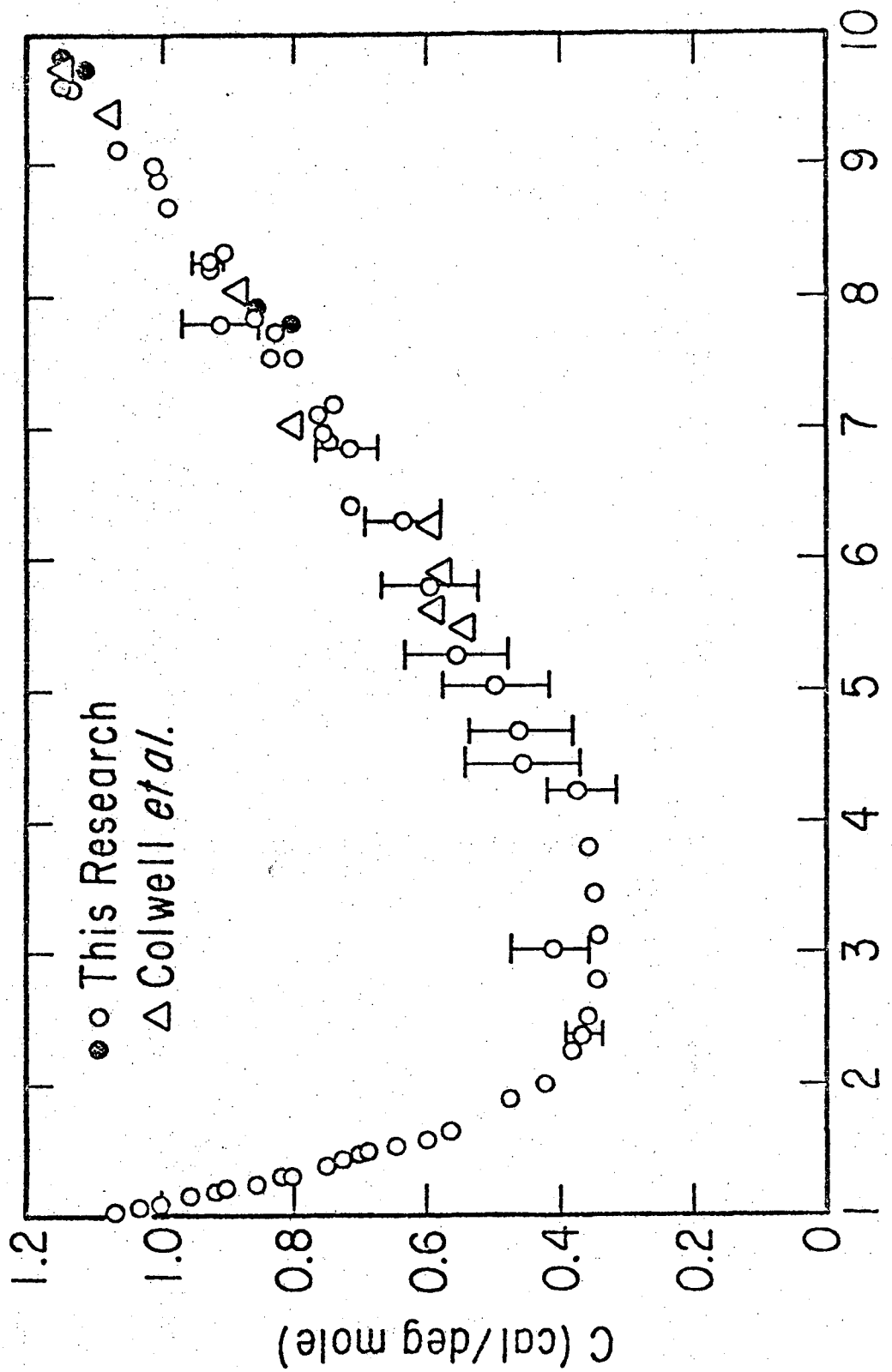

Figure 5. Equilibrium heat capacity of methane from 1 to 10°K. Open circles are for methane doped with oxygen; solid circles for pure methane.

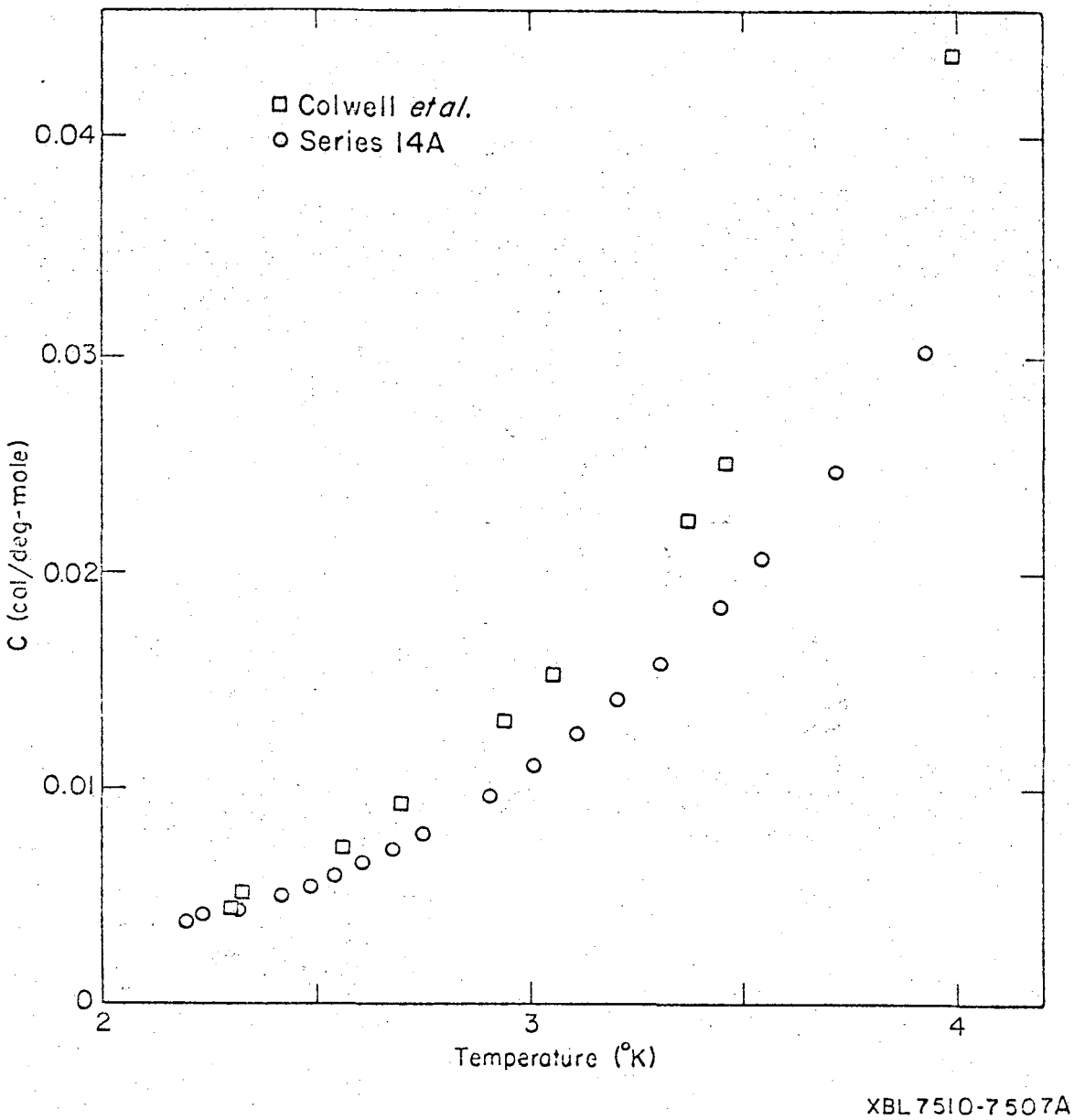

Figure 4. Non-equilibrium heat capacity of methane (with frozen spin-species composition) from 2 to 4°K.

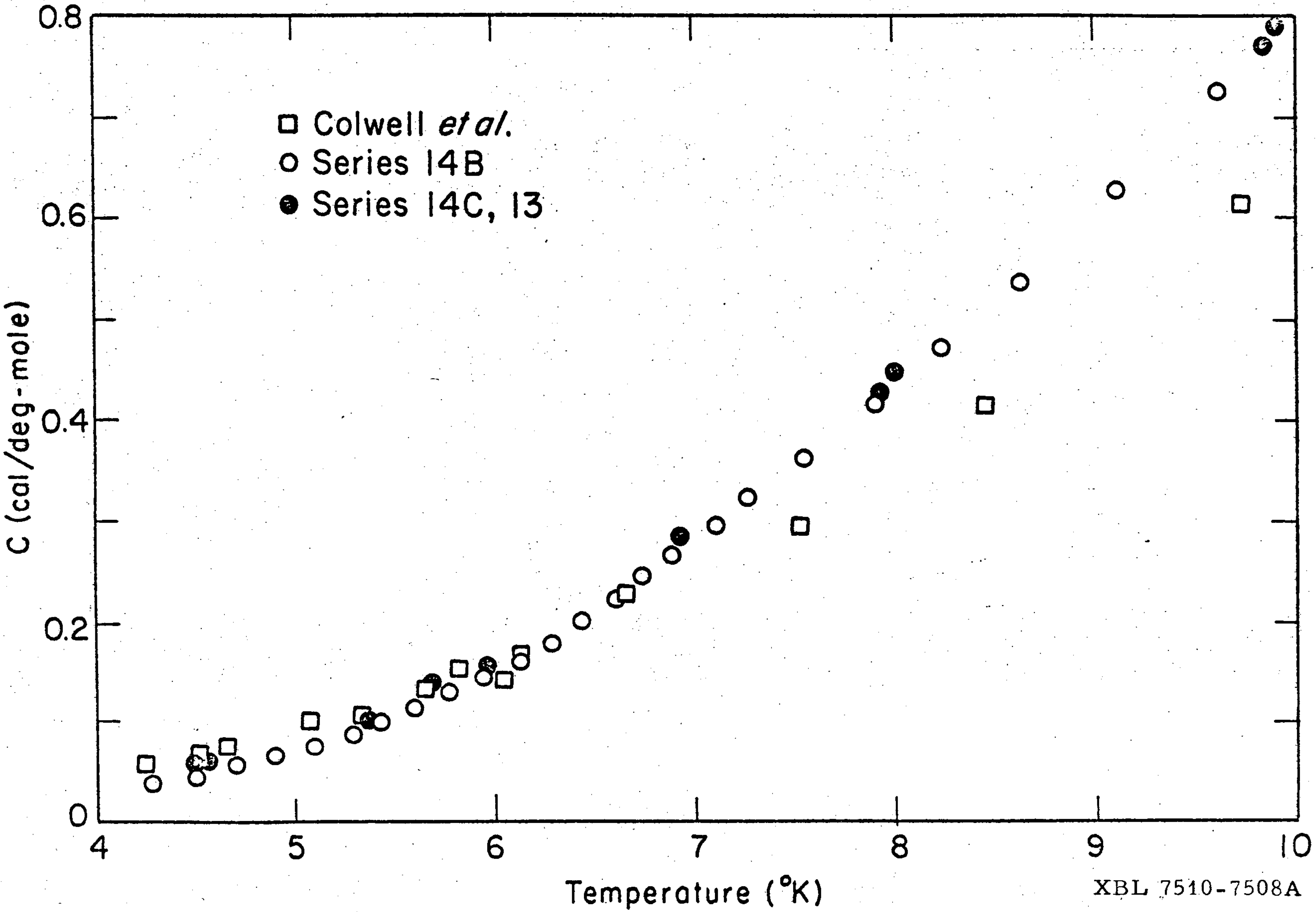

XBL 7510-7508A

Figure 5. Non-equilibrium heat capacity of methane from 4 to 10°K; see text for discussion of spin-species composition for various measurements.

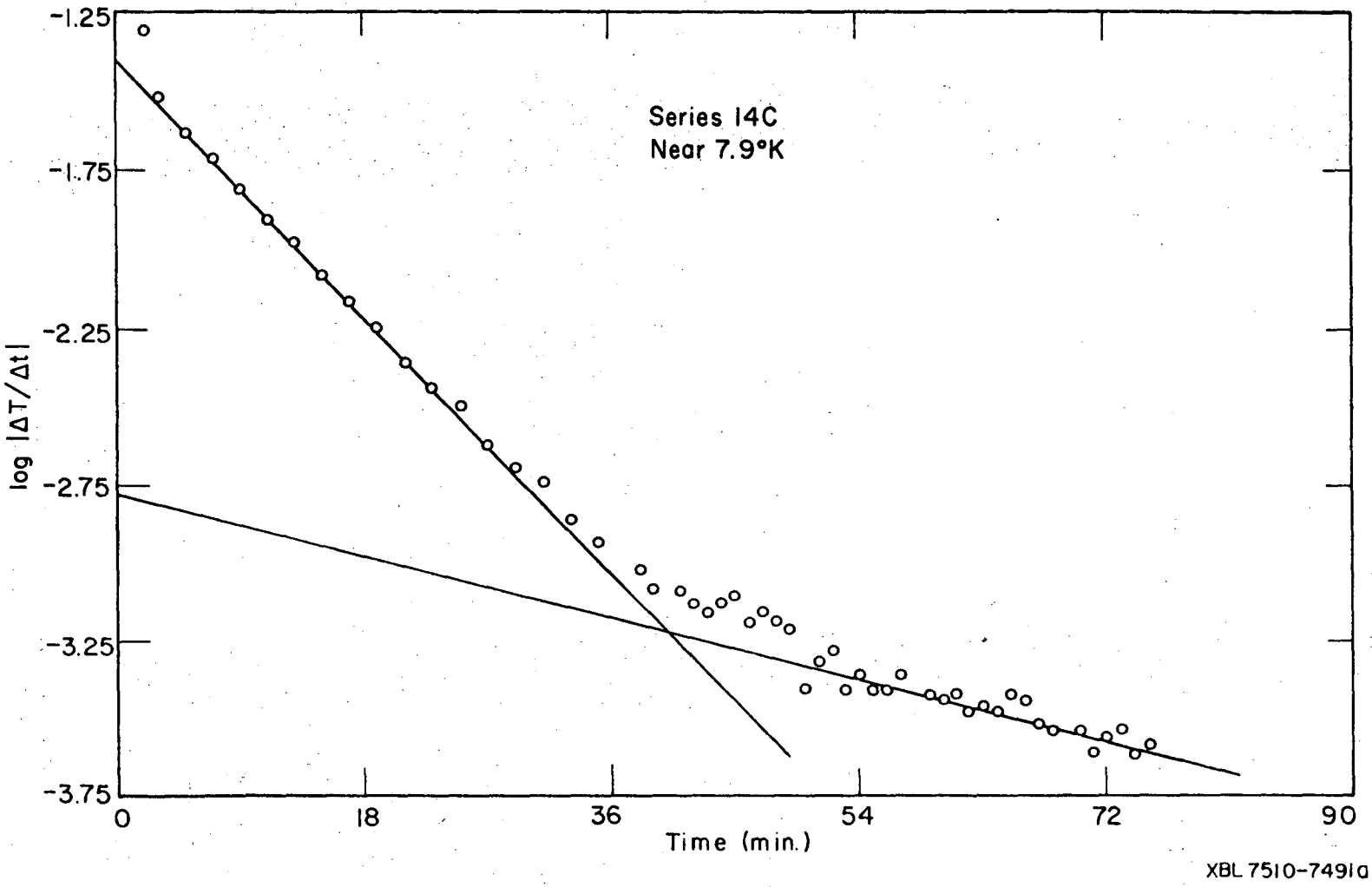

Figure 6. After drifts showing two regions where log ($\Delta T/\Delta t$) is linear in time.

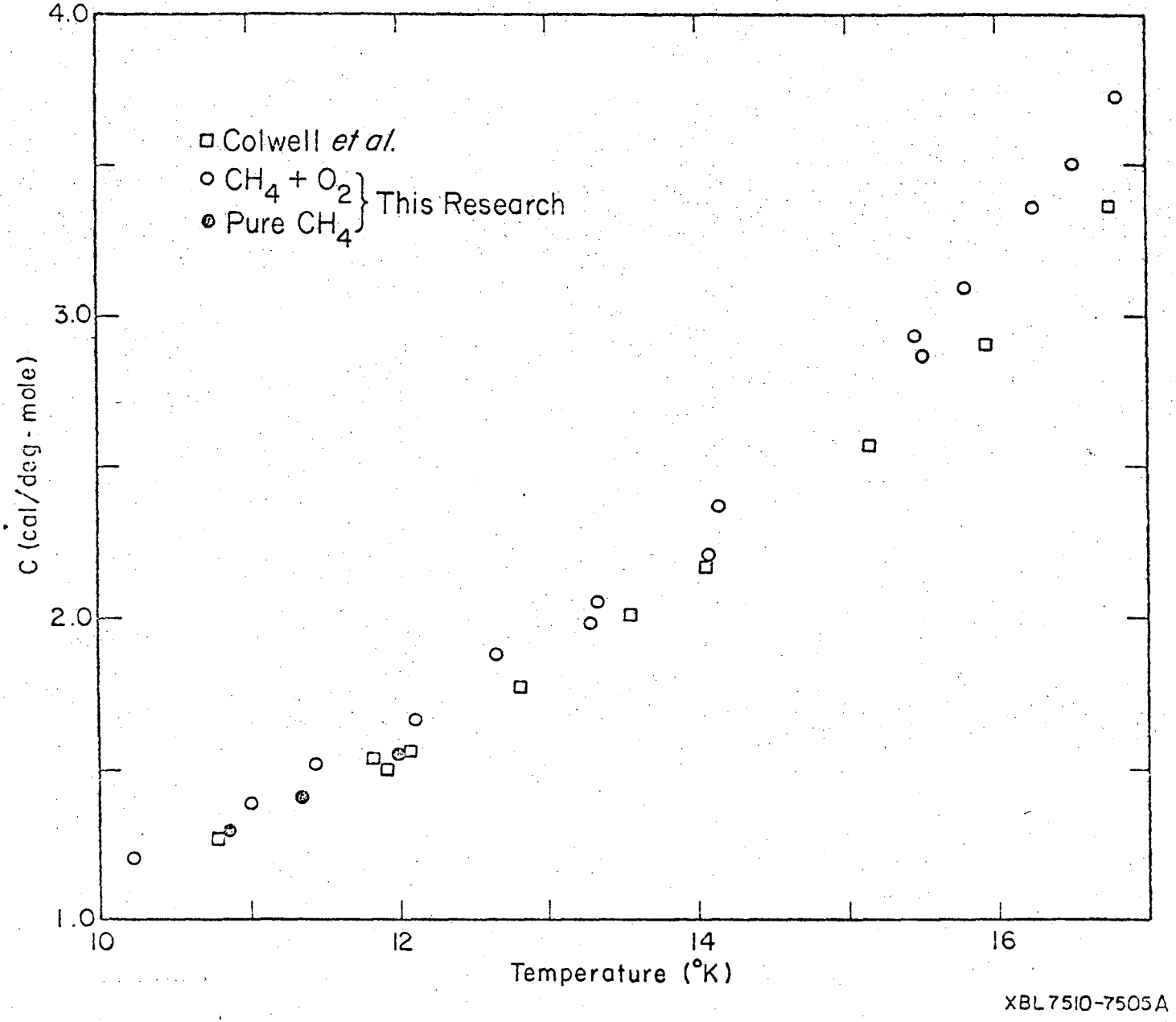

Figure 7. Equilibrium heat capacity of methane from 10 to 17°K.

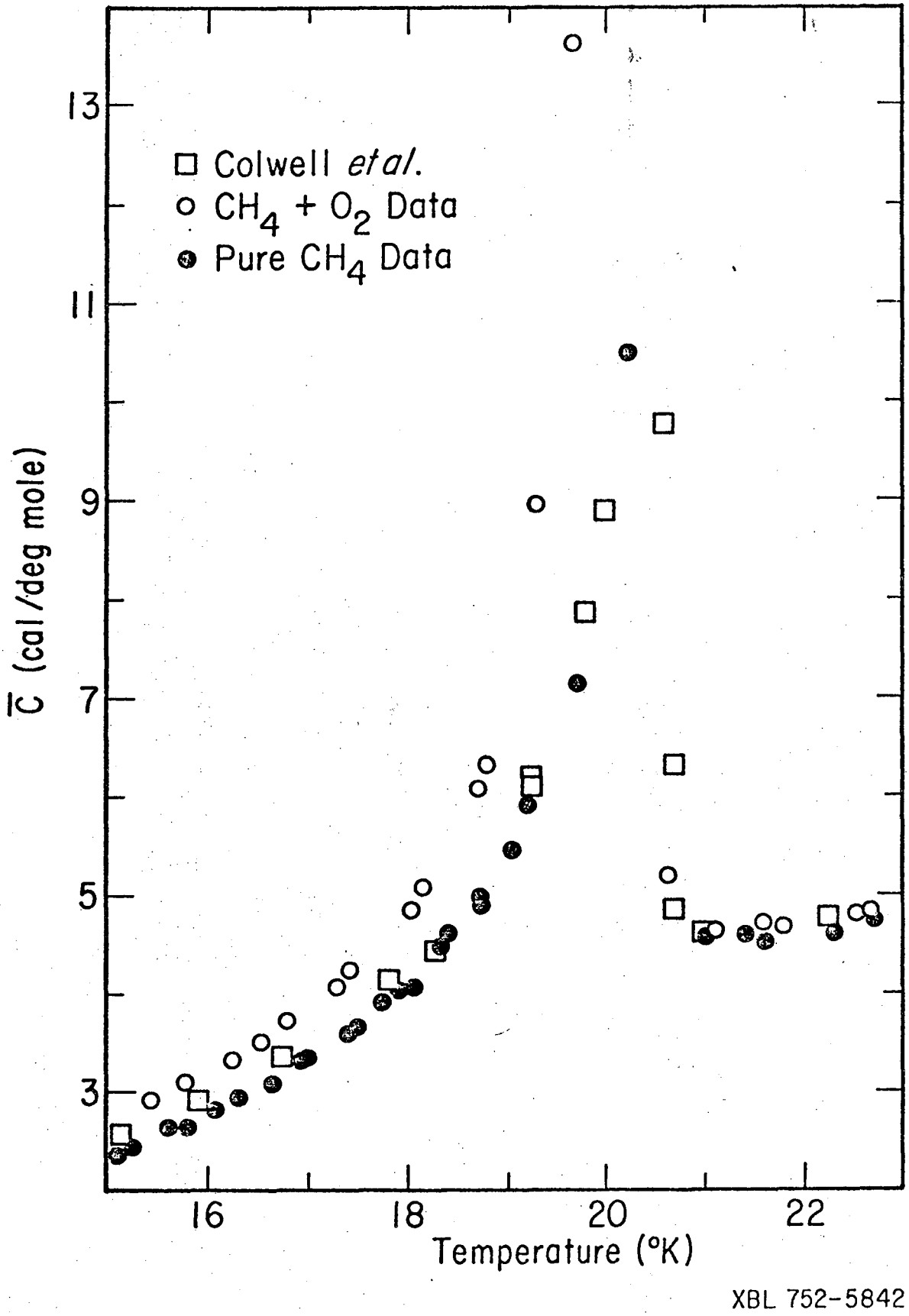

Figure 8. Heat capacity of methane in the region of the transition near 20° K.

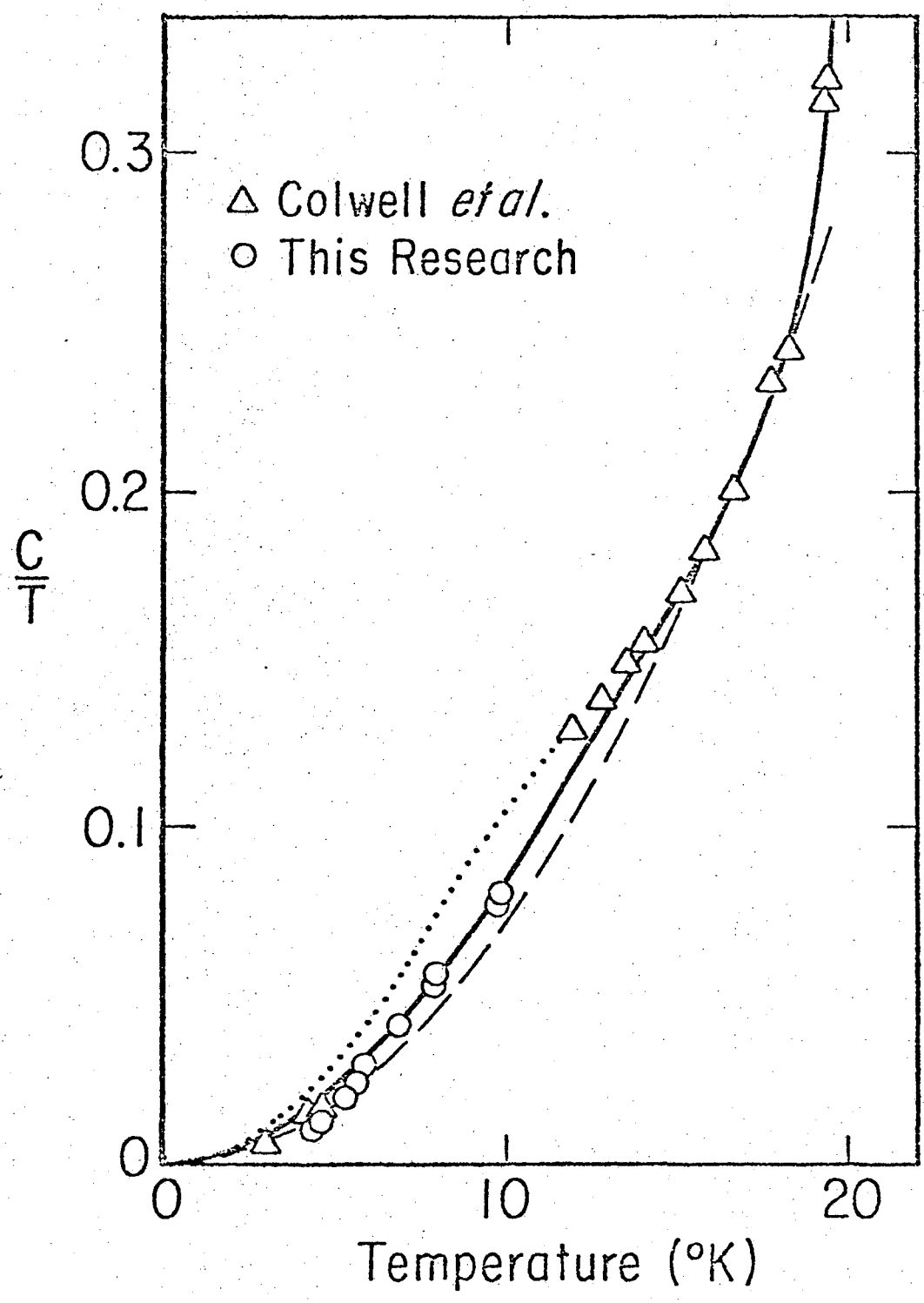

Figure 9. Entropy for non-equilibrium methane from C/T vs T plot; see text for explanation of various curves.

TECHNICAL INFORMATION DIVISION
LAWRENCE BERKELEY LABORATORY
UNIVERSITY OF CALIFORNIA
BERKELEY, CALIFORNIA 94720